

Deterministic quantum computation with one photonic qubit

M. Hor-Meyll, D. S. Tasca, S. P. Walborn, and P. H. Souto Ribeiro*

Instituto de Física, Universidade Federal do Rio de Janeiro, Caixa Postal 68528, Rio de Janeiro, Rio de Janeiro, 21941-972, Brazil

M. M. Santos†

Instituto de Física, Universidade Federal de Uberlândia, Caixa Postal 593, 38400-902, Uberlândia, Minas Gerais, Brazil

E. I. Duzzioni

*Instituto de Física, Universidade Federal de Uberlândia, Caixa Postal 593, 38400-902, Uberlândia, Minas Gerais, Brazil
and Departamento de Física, Universidade Federal de Santa Catarina, Caixa Postal 476, 88040-900, Florianópolis, Santa Catarina Brazil*

(Received 6 March 2015; published 31 July 2015)

We show that deterministic quantum computing with one qubit (DQC1) can be experimentally implemented with a spatial light modulator, using the polarization and the transverse spatial degrees of freedom of light. The scheme allows the computation of the trace of a high-dimension matrix, being limited by the resolution of the modulator panel and the technical imperfections. In order to illustrate the method, we compute the normalized trace of unitary matrices and implement the Deutsch-Jozsa algorithm. The largest matrix that can be manipulated with our setup is 1080×1920 , which is able to represent a system with approximately 21 qubits.

DOI: [10.1103/PhysRevA.92.012337](https://doi.org/10.1103/PhysRevA.92.012337)

PACS number(s): 03.67.Ac, 42.50.Xa, 42.50.Dv, 03.65.Ud

I. INTRODUCTION

Research into the field of quantum information has been strongly motivated by the demonstration that some quantum algorithms have improved performance in comparison to their classical versions. More recently, the deterministic quantum computation with one quantum bit (DQC1) model was introduced with the aim of exploring the computational speedup in high-temperature ensemble quantum computation [1]. Although this model of computation is not universal, it enables quantum speedup to solve certain problems, such as the Shor factorization algorithm [2], the measurement of the average fidelity decay of a quantum map [3], the trace calculus of an arbitrary unitary evolution [4], and the approximation of the Jones polynomial [5]. The importance of the DQC1 model of computing is that it requires little or no entanglement between the qubits of the system [6] to evaluate the trace of a unitary operator, an operation that is not efficiently implemented by a classical computer [4]. The experimental implementation of this model of computation has already been made in optical systems [7] and nuclear magnetic resonance [8,9].

We present an experimental scheme for the implementation of the DQC1 protocol in an optical scenario. In this paradigmatic model, the normalized trace of a unitary matrix is computed by using the computational power of only one qubit in a pure state and a collection of qubits in a completely mixed state. The information about the normalized trace of the unitary matrix is transferred to the qubit state through conditional operations. For this purpose we use a phase-only spatial light

modulator (SLM), which performs polarization-controlled position-dependent phase shifts. Proper polarization measurements return the result of the computation. A similar approach was recently used to demonstrate the use of a SLM and polarized light to estimate integrals [10]. In addition to several possible applications of the SLM [11] and its use as a quantum channel acting on the polarization [12], here we are interested in the implementation of quantum algorithms. Some quantum algorithms have already been implemented or simulated using the SLM, such as the Deutsch algorithm [13], Deutsch-Jozsa algorithm [14,15], the Grover algorithm [15], and the quantum walk [16]. Moreover, there has been an implementation of the Deutsch algorithm for two qubits encoded in an optical system using an operation controlled by polarization [17], but there an interferometer was needed to control the spatial mode.

In order to illustrate the implementation of our method, some examples of trace calculation are presented for a few types of matrices and also the realization of the Deutsch-Jozsa algorithm. The oracle function is prepared in the SLM as a matrix of adjustable dimension, up to its resolution limits. For instance, for our high-definition (HD) panel and using full resolution of 1080×1920 pixels, we could implement an oracle function with approximately 2^{21} input values, which would correspond to an input composed of 21 qubits. We show that the performance of the method in the present realization is limited by polarization dephasing effects [12], and other sources of noise like fluctuations in the phase modulation and photon number statistics.

II. DQC1 USING A PHOTONIC QUBIT

We start the discussion by explaining how we can use the SLM to implement the DQC1 circuit as sketched in Fig. 1. We use a light beam with a given transverse wavefront profile as the system $\rho = \rho_t$, and its polarization state as the control qubit. The initial photonic state can be described by

$$\rho_i = |+\rangle\langle+| \otimes \rho_t, \quad (1)$$

*Present address: Departamento de Física, Universidade Federal de Santa Catarina, Caixa Postal 476, 88040-900, Florianópolis, SC Brazil; phsr@if.ufsj.br

†Present address: Instituto de Ciência, Engenharia e Tecnologia, Universidade Federal dos Vales do Jequitinhonha e Mucuri, Rua do Cruzeiro 01, Jardim São Paulo, 39803-371, Teófilo Otoni, Minas Gerais, Brazil.

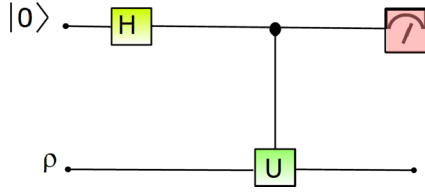


FIG. 1. (Color online) DQC1 circuit. The action of the Hadamard gate on the state $|0\rangle$ gives the state $|+\rangle = (|0\rangle + |1\rangle)/\sqrt{2}$, while the controlled unitary transformation U acts on the state ρ .

where the polarization state $|+\rangle = (|0\rangle + |1\rangle)/\sqrt{2} \equiv (|H\rangle + |V\rangle)/\sqrt{2}$, with $|H\rangle$ ($|V\rangle$) representing the linear horizontal (vertical) polarization state and the state of the transverse wavefront is described by ρ_t .

Both the polarization and the transverse wavefront are properties of the same light beam. It is convenient to describe the wavefront in terms of a discrete basis:

$$\rho_t = C \sum_{i,j} |x_i, y_j\rangle \langle x_i, y_j|, \quad (2)$$

where each state of the basis describes the wavefront in a surface given by the pixel area of the SLM and C is a normalization constant. The SLM will be used to implement the controlled operation. x_i and y_j are the coordinates of pixel i, j . Notice that in this description the state of the wavefront is maximally mixed. We will discuss later how this state can be obtained experimentally.

Let us define an operator describing the action of the SLM on states of the form given by Eq. (1) as [18]

$$S = |H\rangle \langle H| \otimes U + |V\rangle \langle V| \otimes \mathbb{1}, \quad (3)$$

where

$$U = \sum_{i,j} e^{-i\phi(x_i, y_j)} |x_i, y_j\rangle \langle x_i, y_j|, \quad (4)$$

and $\phi(x_i, y_j)$ is a real function.

The SLM used in our experiment only modulates the horizontal polarization component of the input light beam. The function $\phi(x_i, y_j)$ is programmed to apply a phase between 0 and 2π in each SLM pixel located at (x_i, y_j) .

We use Eqs. (1)–(3) to obtain the photonic state after incidence on the SLM:

$$\begin{aligned} \rho_f &= S \rho_i S^\dagger = S[|+\rangle \langle +| \otimes \rho_t] S^\dagger \\ &= (1/2)(|H\rangle \langle H| U \rho_t U^\dagger + |V\rangle \langle V| \rho_t \\ &\quad + |H\rangle \langle V| U \rho_t \mathbb{1} + |V\rangle \langle H| \mathbb{1} \rho_t U^\dagger), \end{aligned} \quad (5)$$

and using the decompositions in Eqs. (2) and (4), we calculate the partial trace over the spatial degrees of freedom:

$$\begin{aligned} \rho_{\text{pol}} \equiv \text{Tr}_t[\rho_f] &= \frac{1}{2} \left(|H\rangle \langle H| + |V\rangle \langle V| \right. \\ &\quad + |H\rangle \langle V| C \sum_{i,j} e^{-i\phi(x_i, y_j)} \\ &\quad \left. + |V\rangle \langle H| C \sum_{i,j} e^{+i\phi(x_i, y_j)} \right). \end{aligned} \quad (6)$$

In terms of matrix representation the state can be written in the basis $\{|H\rangle, |V\rangle\}$ as

$$\rho_{\text{pol}} = \frac{1}{2} \begin{pmatrix} 1 & C \sum_{i,j} e^{-i\phi(x_i, y_j)} \\ C \sum_{i,j} e^{+i\phi(x_i, y_j)} & 1 \end{pmatrix}. \quad (7)$$

This result shows that the information about the spatial modulation is transferred to the coherences of the polarization state, in terms of the average of the modulation distribution. Therefore, the expectation value $\langle \sigma_x \rangle$ of the Pauli operator σ_x for this state gives

$$\langle \sigma_x \rangle = C \sum_{i,j} \cos[\phi(x_i, y_j)], \quad (8)$$

which is the sum over the real parts of the modulation phases. We also have access to the sum over the imaginary parts of the modulation phases through the measurement of σ_y :

$$\langle \sigma_y \rangle = C \sum_{i,j} \sin[\phi(x_i, y_j)]. \quad (9)$$

We can interpret the modulation phases $e^{-i\phi(x_i, y_j)}$ for each pixel as the diagonal elements of a matrix. Therefore, our scheme provides a method for calculating the normalized trace of this matrix through the measurement of $\langle \sigma_x \rangle$ and $\langle \sigma_y \rangle$.

A. Implementation of the Deutsch-Jozsa algorithm

To illustrate further utility of the scheme, let us consider the implementation of the Deutsch-Jozsa algorithm. In this paradigmatic quantum algorithm, one wishes to test if an oracle function is constant or balanced [19]. The oracle function is implemented on the SLM. In the simplest case, also known as the Deutsch algorithm [20], the SLM surface is divided in only two equal parts, where the upper part is given by $y_j \geq 0$ and the lower part is given by $y_j < 0$. This corresponds to dimension $d = 2$, as illustrated in Fig. 2.

For this algorithm, we use only two possible modulation phases for each half of the SLM: 0 or π . For $\phi(x_i, y_j) = 0$,

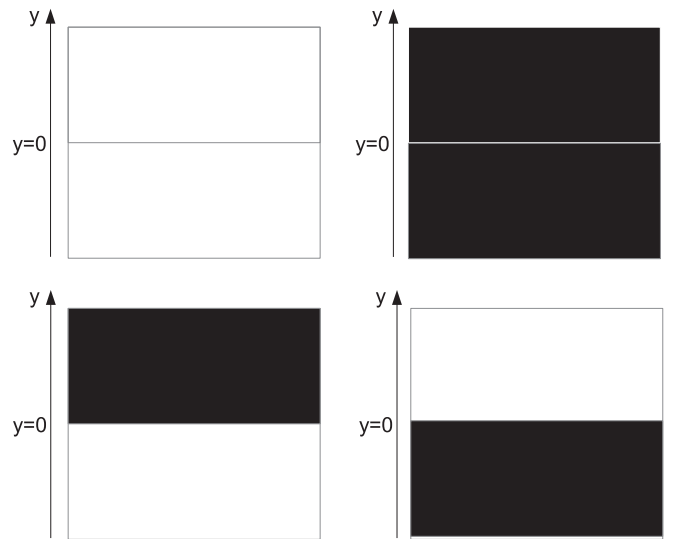


FIG. 2. Representation of the possible modulations for $d = 2$. White corresponds to modulation phase 0, and black corresponds to phase π .

$\langle \sigma_x \rangle = +1$, and for $\phi(x_i, y_j) = \pi$, $\langle \sigma_x \rangle = -1$. Therefore, for a constant function we have $\langle \sigma_x \rangle = \pm 1$ and for a balanced function we have $\langle \sigma_x \rangle = 0$.

The algorithm is easily generalized (Deutsch-Jozsa algorithm) to any desired number of divisions of the SLM surface, up to the limit of a single pixel per division. In this case, we can have $1080 \times 1920 = 2\,073\,600$ cells that could be programmed individually with 0 or π . This is equivalent to testing a function with an input of approximately 21 qubits. The expected result for the Deutsch-Jozsa algorithm is the same as for two divisions, meaning that every kind of modulation map that modulates half of the surface with 0 and half with π implements a balanced function and should return zero as result.

III. EXPERIMENT

The experimental setup is sketched in Fig. 3. A helium-cadmium (He-Cd) laser oscillating at 325 nm is used to pump a type I Beta Barium Borate (BBO) nonlinear crystal. It produces pairs of photons via parametric down-conversion, and we adjust the phase-matching angle to obtain collinear twin beams at the degenerate wavelength of 650 nm. The down-converted signal and idler beams are separated with a 50:50 beam splitter, and detected using 10-nm bandwidth interference filters placed in front of the detectors. The idler beam is sent directly to a single-photon counter labeled DET1, and the signal beam is sent to a spatial light modulator (SLM) and polarization optics before detection by a single-photon counter labeled DET2. Coincidence detection is used to postselect time-correlated events signaling the arrival of a twin photon pair. In this way, the idler photon at DET1 heralds the presence of the signal photon. The signal photon propagates through L1, which is a lens implementing an optical Fourier transform mapping the far-field distribution in the crystal plane onto the SLM. Using this lens system we avoid much of the free propagation effects of the beams, minimizing unwanted diffraction and transverse spatial cross correlations.

The idler beam also propagates through L1 before splitting in the beam splitter. Its far-field distribution is mapped on an intermediate plane, just like the signal but without an SLM. In our experiment, we use a reflective full HD 1080 \times 1920 pixels, phase-only SLM made by Holoeye Photonics. We are able to

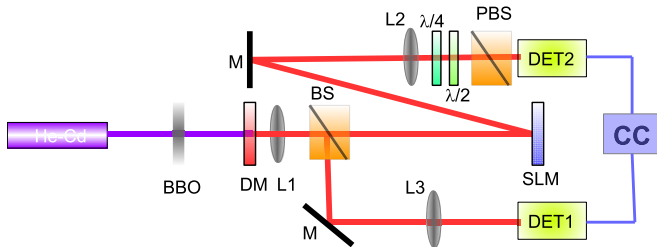


FIG. 3. (Color online) Experimental setup. He-Cd is a helium-cadmium laser; BBO is a nonlinear crystal; DM is a dichroic mirror; M represents mirrors; L1, L2, and L3 are lenses; $\lambda/4$ is a quarter-wave plate; $\lambda/2$ is a half-wave plate; BS is a 50:50 beam splitter; PBS is a polarizing beam splitter; SLM is the spatial light modulator; DET1 and DET2 are single-photon counting modules; and CC is a coincidence detection circuit.

access each pixel individually and program any modulation phase ranging from 0 to 2π . A specific function $\phi(x_i, y_j)$ characterizing the modulation distribution in the plane of the SLM is programmed, and the signal field wavefront acquires this phase conditioned on the polarization. The input beam is prepared in a linearly polarized state along the diagonal direction: $|+\rangle = (|H\rangle + |V\rangle)/\sqrt{2}$, so that the horizontal component is modulated and the vertical is not. After interaction with the SLM, we measure the resulting polarization state given by Eq. (7), in two different bases, obtaining information about the modulation of the spatial profile. Lens L2 forms the image of the SLM surface in the detection plane.

Lens L3 in the idler beam forms the image of the intermediate plane were the far field were mapped previously by L1. In this way, the spatial propagations of signal and idler beams are equivalent, except for the presence of the SLM in the signal. The polarization analysis is made with a quarter-wave plate $\lambda/4$, followed by a half-wave plate $\lambda/2$ and a polarizing beam splitter (PBS). We register both the single-photon and two-photon coincidence counts.

Due to the spatial correlations, depending on how the idler photon is detected, the heralded signal photon can be prepared to have different spatial properties [21]. For a small idler detection area, the heralded signal beam becomes spatially coherent, which means that Eq. (2) is not suitable for describing its transverse wavefront. For a large detection area of the idler photon, the heralded signal beam is spatially incoherent, and is well described by Eq. (2). The use of twin

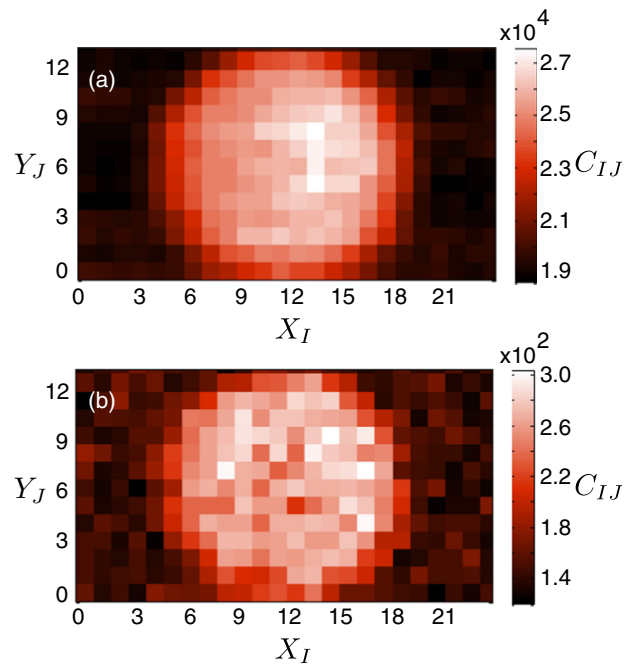


FIG. 4. (Color online) Transverse profile of the beam on the SLM. (a) Single-photon counting distribution (counts/s). (b) Coincidence counting rate (coincidences/s). The transverse coordinates X_I and Y_J refer to the coordinates of detection cells containing an array of (80×80) pixels. C_{IJ} is the single-coincidence counting rate in the cell located at (X_I, Y_J) .

photons and coincidence detection thus allows the preparation of states with controllable purity.

It is important to characterize the spatial intensity distribution of the light beam interacting with the SLM panel, as it may have some influence on the computation. Figure 4 shows the intensity profile of the signal light beam used, already triggered by the idler. This profile will be taken into account in the calculation of the trace of a matrix using our scheme.

IV. RESULTS

A. Implementation of the Deutsch-Jozsa algorithm

We begin by presenting the results obtained in the implementation of the Deutsch-Jozsa algorithm, as it is a special (and simpler) case of the general calculation of the normalized trace of a matrix. In Fig. 5 we show the surface modulation of the SLM and the measured values of $\langle\sigma_x\rangle$. For the constant functions the ideal value should be $\langle\sigma_x\rangle = +1$ for $\phi = 0$ and

$\langle\sigma_x\rangle = -1$ for $\phi = \pi$, and we observe a good agreement with the measurements. For the balanced functions, we apply SLM masks with half of the cells modulated with $\phi = 0$ and half with $\phi = \pi$ distributed randomly on the SLM surface. The randomness reduces the need for a precise knowledge of the spatial distribution of the light beam on the surface of the SLM. The results are shown in Fig. 5 for square cells containing (1×1) , (5×5) , and (10×10) pixels. We can see that for all resolutions the measured value of $\langle\sigma_x\rangle$ is very close to zero, showing that the algorithm works well even when using the full resolution of the SLM. For the purpose of deciding if the oracle function is constant or balanced, a relatively high degree of uncertainty is tolerated, since one is required to discriminate between 0 and ± 1 . However, it is also clear that the error is smaller for larger sizes of the modulation cell, indicating the presence of unwanted noise effects, like residual diffraction, for instance.

B. Computation of the normalized trace of a matrix

As we can see from the results in Eq. (6), we can implement the DQC1 model for a general function programmed in the SLM, where we can define squares or other geometries composed by an arbitrary number of pixels and modulate each one with some arbitrary phase ranging from 0 to 2π . The measurement of $\langle\sigma_x\rangle$ gives the real part of the sum over all phases, and $\langle\sigma_y\rangle$ gives the imaginary part. Therefore, the system is able to perform the calculation of the trace of a normalized matrix imprinted in the SLM. In this case, it is not only a matter of determining if the function is balanced or constant, but rather of obtaining a result that is as precise as possible.

In order to illustrate the method, we programmed the SLM panel with phases varying linearly along the y direction, according to

$$\phi(x_i, y_j) = \phi_0 + \frac{y_j}{N_y} \phi_f, \quad (10)$$

where $N_y = 1080$ is the number of pixels along the y direction. Thus, the matrix element corresponding to position (x_i, y_j) is $e^{-i\phi(x_i, y_j)}$. We have considered four cases of linear functions of the type given in Eq. (10), namely, with $(\phi_0, \phi_f) = (3\pi/4, 5\pi/4)$, $(\pi, 2\pi)$, $(\pi/2, 3\pi/2)$, and $(\pi/2, \pi)$. The measured values $\langle\sigma_x\rangle_{\text{exp}}$ and $\langle\sigma_y\rangle_{\text{exp}}$ for the real and imaginary part of the trace of the corresponding matrices, respectively, are shown in Fig. 6 and summarized in Table I.

We compared the experimental values $\langle\sigma_x\rangle_{\text{exp}}$ and $\langle\sigma_y\rangle_{\text{exp}}$ with a theoretical prediction that takes into account the nonuniform intensity distribution of the light on the SLM panel combined with the unavoidable dephasing effect that is inherent to our Holoeye modulator, as described in detail in Ref. [12]. The theoretical prediction for the real and imaginary parts of the trace of the matrix is well described by

$$\langle\sigma_x\rangle_{\text{theo}} = (1 - 2p) \sum_{i=1}^{N_x} \sum_{j=1}^{N_y} c_{ij} \cos[\phi(x_i, y_j)], \quad (11)$$

$$\langle\sigma_y\rangle_{\text{theo}} = (1 - 2p) \sum_{i=1}^{N_x} \sum_{j=1}^{N_y} c_{ij} \sin[\phi(x_i, y_j)],$$

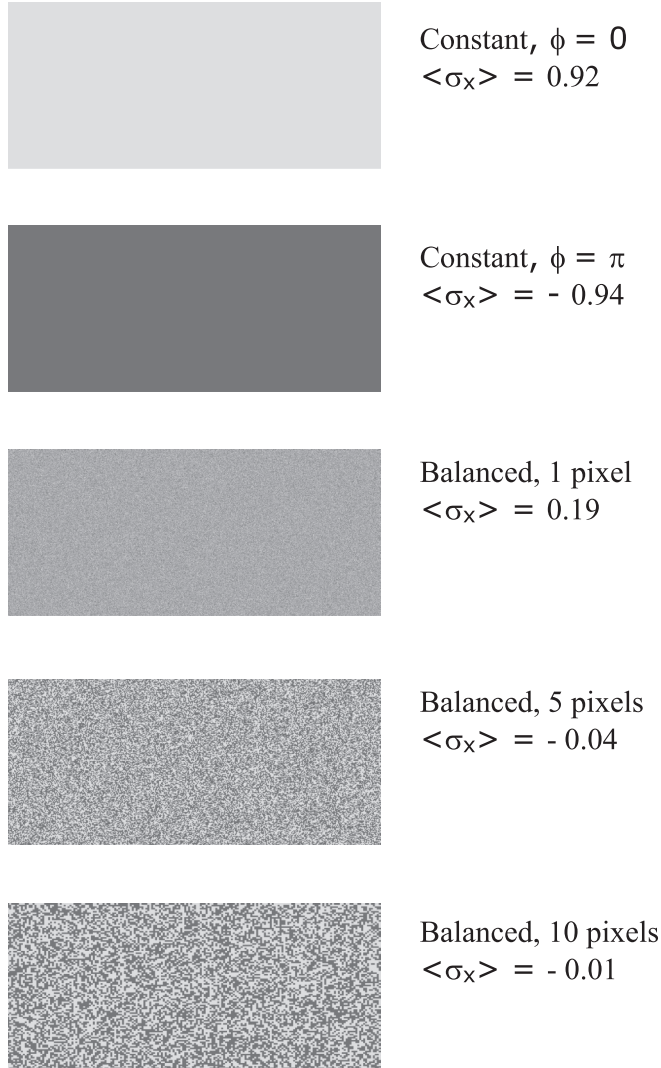


FIG. 5. Images displayed on the SLM panel for constant and balanced functions and the respective measured values of $\langle\sigma_x\rangle$. The balanced functions are implemented through (1×1) , (5×5) , and (10×10) square pixels cells randomly distributed on the panel.

TABLE I. Experimental and theoretical results for the computation of the traces of the matrices defined by Eq. (10).

(ϕ_0, ϕ_f)	$(\frac{3\pi}{4}, \frac{5\pi}{4})$	$(\pi, 2\pi)$	$(\frac{\pi}{2}, \frac{3\pi}{2})$	$(\frac{\pi}{2}, \pi)$
$\langle \sigma_x \rangle_{\text{exp}}$	-0.811	-0.039	-0.646	-0.579
$\delta_{\langle \sigma_x \rangle}$	± 0.005	± 0.008	± 0.006	± 0.007
$\langle \sigma_x \rangle_{\text{theo}}$	-0.773	0.002	-0.593	-0.548
$\text{Re}[\text{Tr}_n(M)]$	-0.903	-0.004	-0.644	-0.638
$\langle \sigma_y \rangle_{\text{exp}}$	0.007	-0.628	-0.034	0.521
$\delta_{\langle \sigma_y \rangle}$	± 0.008	± 0.007	± 0.008	± 0.007
$\langle \sigma_y \rangle_{\text{theo}}$	0.008	-0.587	-0.009	0.545
$\text{Im}[\text{Tr}_n(M)]$	0.012	-0.637	-0.003	0.639

where p is a parameter which gives the degree of dephasing and c_{ij} is the measured intensity of the light incident on the SLM pixel at position (x_i, y_j) . The overall dephasing effect is to decrease the coherences in Eq. (7) by a factor of $(1 - 2p)$. According to Ref. [12], the estimated value for p , considering the specific modulator we are using, is 0.08 ± 0.02 . We determine c_{ij} from the measurement of the transverse profile of the beam, shown in Fig. 4(b). The resolution of our measurement of the beam transverse intensity is set by the size of a square cell composed by 80×80 pixels. Assuming a flat intensity distribution within the cell at position (X_I, Y_J) , the intensity c_{ij} on a pixel at position (x_i, y_j) inside the cell can be approximated by

$$c_{ij} = \frac{1}{N} \frac{C_{IJ}}{80 \times 80}, \quad (12)$$

where C_{IJ} is the coincidence counts for the corresponding cell and N is a normalization factor given by

$$N = \sum_{I=1}^{N_x/80} \sum_{J=1}^{N_y/80} C_{IJ}, \quad (13)$$

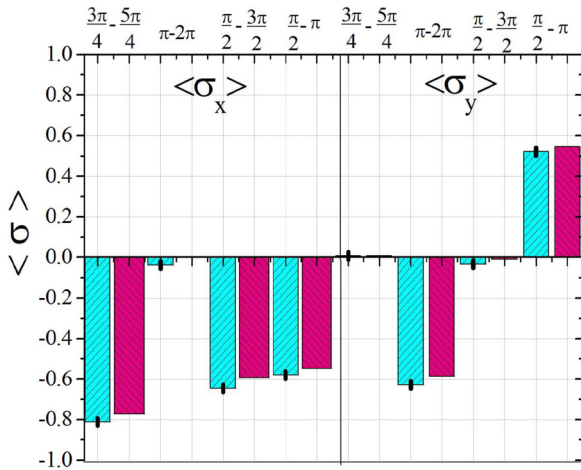


FIG. 6. (Color online) Experimental and theoretical results for the traces of the matrices defined by Eq. (10). Columns filled with forward-diagonal lines (blue [gray]) represent experimental results of measurements of $\langle \sigma_x \rangle$ (left side) and $\langle \sigma_y \rangle$ (right side), and columns filled with backward-diagonal lines (red [gray]) represent theoretical results. The modulation ranges are displayed on the top.

so that

$$\sum_{i=1}^{N_x} \sum_{j=1}^{N_y} c_{ij} = 1. \quad (14)$$

For the sake of completeness, the purely theoretical values for the real and imaginary parts of the normalized trace of matrix M ($\text{Tr}_n(M)$), supposing the transverse field distribution to be flat in the entire SLM panel and disregarding the dephasing effect [12], given by

$$\text{Tr}_n(M) \equiv \text{Tr}(M)/(N_x \cdot N_y), \quad (15)$$

are also shown in Table I.

The error bars of the experimental values, shown in Table I, were computed considering the error in the phase modulation to be equal to the smallest modulation step, which is $\delta\phi \simeq 2\pi/256$, and considering the error in the intensity of the light in the SLM given by the uncertainty of the photon number distribution, considered to be Poissonian, so that $\delta c_{ij} \simeq \sqrt{c_{ij}}$. In general, we have a rather good agreement between experimental and theoretical values within the technical limitations. For instance, they are related to the intrinsic discretization of the modulator (here, we refer to the 256 levels of phase modulation), diffraction, inhomogeneities in the optical beam profile, and imperfections of the optical devices such as wave plates and polarizing beam splitters. Nevertheless, the results serve as a successful proof of principle.

V. CONCLUSION

In conclusion, we present an experiment in which the DQC1 quantum computation model is implemented using a polarization-controlled spatial light modulator (SLM) acting on the wavefront of single-photon fields. We illustrate the utility of the system by implementing the Deutsch-Jozsa algorithm on a system whose size is the equivalent of about 20 qubits using a matrix of 960×960 . The resolution of the SLM allows for the representation of the equivalent of up to about 21 qubits. We also show that a more general calculation is possible and experimentally compute, through polarization measurements, the normalized trace of a matrix whose diagonal elements are represented by modulation phases.

A future path to improve our results concerns the use of alternative optical devices that could also implement polarization controlled operations on the transverse spatial degrees of freedom of photons with better performance. One possibility could be the improvement of the SLM technology or the combined use of multiple SLMs. In this case we might be able to handle much larger matrices.

ACKNOWLEDGMENTS

Financial support was provided by Brazilian agencies CNPq, CAPES, FAPERJ, and the National Institute of Science and Technology for Quantum Information.

- [1] E. Knill and R. Laflamme, *Phys. Rev. Lett.* **81**, 5672 (1998).
- [2] S. Parker and M. B. Plenio, *Phys. Rev. Lett.* **85**, 3049 (2000).
- [3] D. Poulin, R. Blume-Kohout, R. Laflamme, and H. Ollivier, *Phys. Rev. Lett.* **92**, 177906 (2004).
- [4] Animesh Datta, [arXiv:0807.4490](https://arxiv.org/abs/0807.4490).
- [5] P. W. Shor and S. P. Jordan, *Quant. Inf. Comp.* **8**, 681 (2008).
- [6] A. Datta, S. T. Flammia, and C. M. Caves, *Phys. Rev. A* **72**, 042316 (2005).
- [7] B. P. Lanyon, M. Barbieri, M. P. Almeida, and A. G. White, *Phys. Rev. Lett.* **101**, 200501 (2008).
- [8] C. A. Ryan, J. Emerson, D. Poulin, C. Negrevergne, and R. Laflamme, *Phys. Rev. Lett.* **95**, 250502 (2005).
- [9] R. Marx, A. Fahmy, L. Kauffman, S. Lomonaco, A. Spörl, N. Pomplun, T. Schulte-Herbrüggen, J. M. Myers, and S. J. Glaser, *Phys. Rev. A* **81**, 032319 (2010).
- [10] G. B. Lemos, P. H. S. Ribeiro, and S. P. Walborn, *J. Opt. Soc. Am. A* **31**, 704 (2014).
- [11] See the introduction of Ref. [8].
- [12] G. B. Lemos, J. O. de Almeida, S. P. Walborn, P. H. S. Ribeiro, and M. Hor-Meyll, *Phys. Rev. A* **89**, 042119 (2014).
- [13] B. Marques, M. R. Barros, W. M. Pimenta, M. A. D. Carvalho, J. Ferraz, R. C. Drumond, M. Terra Cunha, and S. Pádua, *Phys. Rev. A* **86**, 032306 (2012).
- [14] J. Vala, Z. Amitay, B. Zhang, S. R. Leone, and R. Kosloff, *Phys. Rev. A* **66**, 062316 (2002).
- [15] G. Puentes, C. La Mela, S. Ledesma, C. Iemmi, J. P. Paz, and M. Saraceno, *Phys. Rev. A* **69**, 042319 (2004).
- [16] D. Francisco, C. Iemmi, J. P. Paz, and S. Ledesma, *Phys. Rev. A* **74**, 052327 (2006).
- [17] A. N. de Oliveira, S. P. Walborn, and C. H. Monken, *J. Opt. B* **7**, 288 (2005).
- [18] M. Hor-Meyll, J. O. de Almeida, G. B. Lemos, P. H. S. Ribeiro, and S. P. Walborn, *Phys. Rev. Lett.* **112**, 053602 (2014).
- [19] D. Deutsch and R. Jozsa, *Proc. R. Soc. London A* **439**, 553 (1992).
- [20] D. Deutsch, *Proc. R. Soc. London A* **400**, 7 (1985).
- [21] S. P. Walborn, S. Padua, C. H. Monken, and P. H. S. Ribeiro, *Phys. Rep.* **495**, 87 (2010).